Role of the Metal Center in the Homogeneous Catalytic Decarboxylation of Select Carboxylic Acids. Copper(I) and Zinc(II) Derivatives of Cyanoacetate

Donald J. Darensbourg,* Matthew W. Holtcamp, Elisabeth M. Longridge, Bandana Khandelwal, Kevin K. Klausmeyer, and Joseph H. Reibenspies

Contribution from the Department of Chemistry, Texas A&M University, College Station, Texas 77843

Received August 17, 1994[⊗]

Abstract: The mechanism by which copper(I) influences the decarboxylation of cyanoacetic acid has been studied comprehensively by means of structural and kinetic investigations. The copper(I) complexes, $[(R_3P)_2CuO_2CCH_2CN]_{1,2}$, have been synthesized from the reaction of copper(I) *n*-butyrate with 1 equiv of cyanoacetic acid and 2 equiv of phosphine. In the case of R = Ph, the complex is shown to be a dimer, both in solution and in the solid state, consisting of two copper(I) centers bridged by two cyanoacetate groups that are bound to copper through both the carboxylate functionality and the nitrogen. On the other hand, for the sterically encumbered phosphine (R = Cy), the complex (**3**) is found by X-ray crystallography to be monomeric and to contain a monodentate carboxylate group. The monodentate nature of the cyanoacetate binding was demonstrated to be a function of the electron-withdrawing ability of the cyanoacetate ligand as revealed by an examination of the solid-state structure of the $(Cy_3P)_2Cu$(butyrate) (**4**) analog, where the more basic butyrate ligand was shown to be bound in a bidentate manner. Both phosphine derivatives of copper(I) cyanoacetate were observed to readily undergo reversible decarboxylation/carboxylation processes as evidenced by their exchange reactions with $^{13}CO_2$. A similar, much slower, exchange reaction with ^{13}C-labeled CO_2 was noted for the $[PPN][O_2CCH_2CN]$ and η^3-$HB(3\text{-}PhPz)_3Zn(O_2CCH_2CN)$ (**5**) salts. These $^{13}CO_2$ exchange processes were found to be first-order in the respective substrate, with the Cy_3P derivative undergoing more rapid exchange than the Ph_3P complex. Furthermore, the phosphine derivatives of copper(I) cyanoacetate were efficient catalysts for the decarboxylation of cyanoacetic acid to afford CH_3CN and CO_2 at rates quite similar to the CO_2 exchange process. These reactions were first-order in copper(I) complexes and zero-order in cyanoacetic acid concentrations below 0.05 M. At higher acid concentrations the reaction was inhibited by cyanoacetic acid due to its complexation with copper(I). Both η^3-$HB(3\text{-}PhPz)_3Zn(O_2CCH_2CN)$ and $[([12]ane_3)Zn(O_2CCH_3)][Ph_4B]$ are effective catalysts as well for the decarboxylation of cyanoacetic acid, with the latter cationic derivative being more active. This difference in catalytic behavior is attributed to the weaker Zn−O bond in the cationic derivative as determined by X-ray crystallography, 1.941 vs 1.912 Å. A mechanism for decarboxylation is proposed which involves CO_2 elimination from a cyanoacetic ligand that is nitrile bound to the metal center, *i.e.*, electrophilic catalysis. Crystal data for **3**: monoclinic space group $P2_1/n$, $a = 10.619(2)$ Å, $b = 20.628(3)$ Å, $c = 18.146(3)$ Å, $\beta = 93.89(1)°$, $Z = 2$, $R = 6.40\%$. Crystal data for **4**: triclinic space group $P\bar{1}$, $a = 9.706(2)$ Å, $b = 10.442(2)$ Å, $c = 22.423(4)$ Å, $\alpha = 97.51(2)°$, $\beta = 92.30(2)°$, $\gamma = 116.22(1)°$, $Z = 2$, $R = 4.91\%$. Crystal data for **5**: triclinic space group $P\bar{1}$, $a = 13.197(2)$ Å, $b = 14.657(2)$ Å, $c = 16.049(3)$ Å, $\alpha = 103.44(1)°$, $\beta = 107.10(1)°$, $\gamma = 92.19(1)°$, $Z = 2$, $R = 4.72\%$.

Introduction

The exploitation of CO_2 as an alternative source of chemical carbon is intimately associated with a better understanding of the organometallic chemistry of this ubiquitous molecule pertinent to catalysis.[1] Central reactions in this chemistry are the insertion of CO_2 into M−H, M−C, and M−O bonds. CO_2 insertion into metal−carbon bonds has been shown to be, in general, irreversible (eq 1), whereas CO_2 insertion into metal−hydrogen and metal−oxygen bonds is reversible (eqs 2 and 3, respectively). However, reversible CO_2 uptake has been

$$MR + CO_2 \rightarrow MO_2CR \quad (1)$$

$$MH + CO_2 \rightleftharpoons MO_2CH \quad (2)$$

$$MOR + CO_2 \rightleftharpoons MO_2COR \quad (3)$$

reported for a select number of copper(I) carboxylates.[2] For example, Tsuda and co-workers have found that reversible CO_2 insertion occurred in $Cu^IC{\equiv}CPh$ and Cu^ICH_2CN in the presence of phosphines.[2a,b] The mechanistic details of this important process were not defined in these early reports because the complexes were difficult to isolate.

While there are few examples of reversible CO_2 insertion involving copper(I) alkyl or aryl species, there are numerous reports in which copper(I) salts have received attention as carboxylic acid decarboxylation reagents.[3] Interestingly, it has been shown that only select carboxylic acids are active toward decarboxylation in the presence of copper(I) catalysts. For instance, Toussaint and co-workers have found that only those

[⊗] Abstract published in *Advance ACS Abstracts*, December 15, 1994.

(1) (a) Darensbourg, D. J.; Kudaroski, R. *Adv. Organomet. Chem.* **1983**, *22*, 129. (b) Braunstein, P.; Matt, D.; Nobel, D. *Chem. Rev.* **1988**, *88*, 747. (c) Behr, A. *Carbon Dioxide Activation by Metal Complexes*; VCH: Weinheim, West Germany, 1988.

(2) (a) Tsuda, T.; Chujo, Y.; Saegusa, T. *J. Chem. Soc., Chem. Commun.* **1975**, *1*, 963. (b) Tsuda, T.; Chujo, Y.; Saegusa, T. *J. Am. Chem. Soc.* **1978**, *100*, 630. (c) Darensbourg, D. J.; Longridge, E. M.; Holtcamp, M. W.; Klausmeyer, K. K.; Reibenspies, J. H. *J. Am. Chem. Soc.* **1993**, *115*, 8839.

0002-7863/95/1517-0318$09.00/0

carboxylic acids that formed resonance-stabilized carbanions would decarboxylate in the presence of copper(I) salts.[3c] At this time it is important to note that both $O_2CC{\equiv}CPh$ and O_2CCH_2CN form stabilized carbanions upon loss of CO_2. Indeed, cyanoacetic acid can be readily decarboxylated by copper(I) catalysts.[3g]

Parallel studies in our laboratory have illustrated that tungsten(0) carboxylates serve as active decarboxylation catalysts for cyanoacetic acid, affording acetonitrile and CO_2 as sole products.[4] These tungsten(0) catalysts were less active than their copper(I) counterparts. In-depth mechanistic studies of the group 6 metal system supported tungsten(0)'s role as an electrophile that induced carbon−carbon bond fission in the $WNCCH_2CO_2^-$ intermediate. Concordant with the proposed mechanism, $W(CO)_5O_2CCH_2CN^-$ was inert toward decarboxylation or $^{13}CO_2$ exchange (eq 4).[4b]

$$W(CO)_5O_2CCH_2CN^- \not\rightleftharpoons W(CO)_5CH_2CN^- + CO_2 \qquad W(CO)_5O_2CCH_2CN^- + {}^{13}CO_2 \not\rightarrow W(CO)_5O_2{}^{13}CCH_2CN^- \qquad (4)$$

As previously mentioned, by way of contrast, copper(I) cyanomethyl undergoes reversible CO_2 insertion in the presence of phosphines.[2a] Relevant to this behavior, we have isolated and completely characterized the triphenylphosphine derivative of copper(I) cyanoacetate, $[(Ph_3P)_2CuO_2CCH_2CN]_2$. Furthermore, we have shown that it undergoes $^{13}CO_2$ exchange and serves as a catalyst precursor for the decarboxylation of cyanoacetic acid.[2c] In addition, active, air-stable zinc(II) catalysts have also been prepared and characterized, and were found to behave in an analogous manner, albeit somewhat slower, to the air-sensitive copper(I) catalysts. The mechanistic aspects of these latter processes are needed in order to explain the *apparent* differences in the tungsten(0) and copper(I) systems and to ascertain copper(I)'s role in decarboxylation processes in general. We report herein a mechanism for decarboxylation consistent with all studies concerning the decarboxylation of cyanoacetic acid by transition metal complexes.

Experimental Section

Methods and Materials. All manipulations were carried out under an inert atmosphere unless otherwise stated. The solvents were freshly distilled prior to use. Triphenylphosphine, tricyclohexylphosphine, tri(2-tolyl)phosphine, neocuproine, zinc acetate, cyanoacetic acid, butyric acid, and butyric anhydride were purchased from Aldrich Chemical Co. and used as received. Cuprous butyrate was prepared from the reduction of cupric butyrate by copper turnings in acetonitrile according to a published procedure.[5] Infrared spectra were recorded on a Mattson 6021 spectrometer with DTGS and MCT detectors. ^1H NMR spectra were recorded on a Varian XL-200 super-conducting high-resolution spectrometer. Elemental analyses were carried out by Galbraith Laboratories Inc.

Synthesis of $[(Ph_3P)_2CuO_2CCH_2CN]_2$, 1. This compound was prepared according to the published procedure using cuprous butyrate (1.0 g), cyanoacetic acid (0.56 g), and triphenylphosphine (3.48 g) in diethyl ether at room temperature.[2c] The resulting white precipitate was filtered, washed with 20 mL of diethyl ether, and dried under vacuum. A 3.56-g amount (80%) of product was obtained. Anal. Calcd for $C_{39}H_{32}CuNO_2P_2$: C, 69.69; H, 4.80. Found: C, 69.96; H, 5.07. IR (CH_2Cl_2, cm^{-1}): $\nu(CO_2)$ 1611 (s), 1370 (w); ν(CN) 2255 (s). IR (KBr, cm^{-1}): $\nu(CO_2)$ 1609 (s), 1373 (w); ν(CN) 2255 (s).

Synthesis of $(Cy_3P)_2CuO_2CCH_2CN$, 3. Cuprous butyrate (1.0 g) and cyanoacetic acid (0.56 g) were loaded in a 50 mL flask. Diethyl ether (20 mL) was cannulated into the mixture, forming a white slurry. The mixture was stirred for an hour under argon. The white precipitate of cuprous cyanoacetate was washed with 3 × 20 mL of diethyl ether. The contents of a 50 mL flask containing tricyclohexylphosphine (3.72 g) in 20 mL of diethyl ether were added *via* cannula to the cuprous cyanoacetate, and the solution was left to stir at −78 °C for an hour. The white precipitate that formed was filtered cold, washed with 2 × 20 mL of cold hexane, and dried under vacuum. A 3.70-g amount (79%) of fine white powder was obtained. Anal. Calcd for $C_{39}H_{68}CuNO_2P_2$: C, 66.16; H, 9.69. Found: C, 66.62; H, 9.75. IR (THF, cm^{-1}): $\nu(CO_2)$ 1635 (s), 1339 (w); ν(CN) 2251 (s). IR (KBr, cm^{-1}): $\nu(CO_2)$ 1628 (s), 1354 (w); ν(CN) 2252 (s).

Recrystallization from a concentrated hexane/diethyl ether solution at −20 °C produced single, colorless crystals suitable for an X-ray structure determination.

Synthesis of $(Cy_3P)_2CuO_2CCH_2CH_2CH_3$, 4. Cuprous butyrate (0.5 g) and tricyclohexylphosphine (2.05 g) were loaded in a 50 mL flask. Diethyl ether (20 mL) was added and left stirring for 2 h at room temperature. The white precipitate obtained was filtered, washed with 3 × 20 mL of hexane, and dried. A 2.0 g amount (89%) of fine white powder was obtained. Anal. Calcd for $C_{40}H_{73}CuO_2P_2$: C, 71.15; H, 5.52. Found: C, 71.08; H, 5.39. IR (THF, cm^{-1}): $\nu(CO_2)$ 1567 (s), 1402 (w).

Recrystallization from a concentrated hexane/diethyl ether solution at −20 °C produced single, colorless crystals suitable for an X-ray structure determination.

Synthesis of $(CH_3C_6H_4)_3PCuO_2CCH_2CN$. This compound was prepared at room temperature in a manner analogous to that of the tricyclohexylphosphine−cuprous cyanoacetate described above using cuprous butyrate (0.5 g), cyanoacetic acid (0.28 g), and tri(2-tolyl)-phosphine (2.02 g). A 1.25-g amount (84%) of white powder was obtained as product. Anal. Calcd for $C_{24}H_{23}CuNO_2P$: C, 63.78; H, 5.13. Found: C, 63.58; H, 5.13. IR (CH_2Cl_2, cm^{-1}): $\nu(CO_2)$ 1640 (s), 1379 (w); ν(CN) 2258 (s). IR (KBr, cm^{-1}): $\nu(CO_2)$ 1640 (s), 1379 (w); ν(CN) 2259 (s).

Synthesis of $(\eta^3$-HB(3-Phpz)$_3)ZnO_2CCH_3{\cdot}H_2O$. Potassium hydrotris(3-phenylpyrazol-1-yl)borate was prepared according to the published procedure.[6] Zinc acetate (1.8 g) and potassium hydrotris-(3-phenylpyrazol-1-yl)borate (3.0 g) were loaded in a 100 mL flask. Tetrahydrofuran (30 mL) was added to the mixture and left to stir at room temperature for 2 h. Addition of 40 mL of water led to the precipitation of the product, which was filtered, washed with 3 × 10 mL of water, washed with hexane, and dried under vacuum. A 3.28-g amount (91%) of compound was obtained. Anal. Calcd for $BC_{29}H_{25}N_6O_2Zn{\cdot}H_2O$: C, 59.67; H, 4.66. Found: C, 60.44; H, 4.99. IR (THF, cm^{-1}): $\nu(CO_2)$ 1605 (s) and ν(B−H) 2484 (s).

Synthesis of $(\eta^3$-HB(3-Phpz)$_3)ZnO_2CCH_2CN$, 5. (η^3-HB(3-Phpz)$_3$)ZnO_2CCH_3 (1.0 g) and cyanoacetic acid (0.21 g) were loaded in a 50 mL flask. Tetrahydrofuran (10 mL) was cannulated into the above mixture which was left to stir at room temperature for 2 h. Addition of 20 mL of hexane led to precipitation. The precipitate was filtered, washed with water (3 × 10 mL), washed with hexane (2 × 10 mL), and dried under vacuum. A 1.0-g amount (87%) of white product was obtained. Anal. Calcd for $BC_{30}H_{24}N_7O_2Zn{\cdot}2H_2O$: C, 57.49; H, 4.50. Found: C, 57.83; H, 4.21. IR (THF, cm^{-1}): $\nu(CO_2)$ 1662 (s), 1651 (s); ν(CN) 2262 (s); and ν(B−H) 2519 (s). IR (KBr, cm^{-1}): ν-(CO_2) 1662 (s), 1649 (s); ν(CN) 2264 (s); and ν(B−H) 2519 (s).

Recrystallization from slow diffusion of hexane into a dichloromethane solution produced single, colorless crystals suitable for an X-ray structure analysis.

(3) (a) Leake, P. H. *Chem. Rev.* **1956**, *56*, 27 and references cited therein. (b) Cairncross, A.; Roland, J. R.; Henderson, R. M.; Sheppard, W. A. *J. Am. Chem. Soc.* **1970**, *92*, 3187. (c) Toussaint, O.; Capdevielle, P.; Maumy, M. *Synthesis* **1986**, 1029. (d) Toussaint, O.; Capdevielle, P.; Maumy, M. *Tetrahedron* **1984**, *40*, 3229. (e) Toussaint, O.; Capdevielle, P.; Maumy, M. *Tetrahedron Lett.* **1987**, *28*, 539. (f) Cohen, T.; Beninger, R. W.; Wood, J. T. *J. Org. Chem.* **1978**, *43*, 837. (g) Darensbourg, D. J.; Longridge, E. M.; Atnip, E. V.; Reibenspies, J. H. *Inorg. Chem.* **1992**, *31*, 3951.

(4) (a) Darensbourg, D. J.; Chojnacki, J. A.; Atnip, E. V. *J. Am. Chem. Soc.* **1993**, *115*, 4675. (b) Darensbourg, D. J.; Joyce, J. A.; Rheingold, A. *Organometallics* **1991**, *10*, 3407.

(5) Edwards, D. A.; Richards, R. J. *J. Chem. Soc., Dalton Trans.* **1973**, 2463.

(6) Trofimenko, S.; Calabrese, J. C.; Thompson, J. S. *Inorg. Chem.* **1987**, *26*, 1507.

Catalytic Decarboxylation of Cyanoacetic Acid. The catalytic decarboxylation of cyanoacetic acid to form acetonitrile and CO_2 using phosphine copper carboxylates as catalysts was observed by infrared spectroscopy in a tetrahydrofuran solution. In a typical experiment, a solution of cyanoacetic acid (0.020 g) in tetrahydrofuran (5.0 mL) was transferred via cannulation to a flask containing a 5-mL solution of copper cyanoacetate (0.040 g) and 2 equiv of phosphine. The flasks were warmed to 40 °C prior to cannulation and were maintained at this temperature throughout the experiment. The disappearance of the strong $\nu(CO_2)$ band of the acid at 1745 cm^{-1} was observed with concomitant appearance of the $\nu(CN)$ band of acetonitrile at 2259 cm^{-1} and the $\nu(CO_2)$ band of CO_2 at 2336 cm^{-1}.

The kinetic rates of less active catalysts such as (η^3-HB(3-Phpz)$_3$)ZnO_2CCH_2CN and [PPN][O_2CCH_2CN] were done in an analogous manner at 55.4 °C.

The kinetics of the catalytic decarboxylation of HO_2CCH_2CN were monitored by infrared spectroscopy. Solution temperatures were controlled by a thermostated water bath with a precision of ±0.1 °C. Small aliquots of solution (~0.2 mL) were withdrawn periodically by a syringe and examined by IR. The rate of catalysis was monitored by following the disappearance of the $\nu(CO_2)$ band of the acid at 1745 cm^{-1}. A base-line correction was made on each spectrum by subtracting the absorbance in a region free of any peaks. This value was arbitrarily chosen as 2200 cm^{-1}. Rate constants were determined from the slope of a plot of A/A_0 vs time where A_0 is the initial absorbance at 1745 cm^{-1} for time, $t = 0$, and A is intensity at 1745 cm^{-1} at a time, t. A linear plot was obtained throughout the course of the reaction.

$^{13}CO_2$ Exchange with $(Cy_3P)_2CuO_2CCH_2CN$. Cuprous cyanoacetate (0.04 g) and tricyclohexylphosphine (0.148 g) were loaded in a 25 mL flask. Tetrahydrofuran (3 mL) was introduced into the mixture (catalyst concentration at 0.0892 M), and a $^{13}CO_2$ atmosphere was placed over it. The solution was maintained at 20 °C. The $^{13}CO_2$ exchange rate data were collected by following the disappearance of $\nu(CO_2)$ asymmetric stretch at 1635 cm^{-1} and simultaneous appearance of $\nu(^{13}CO_2)$ infrared band at 1595 cm^{-1}.

Experiments were performed with varied concentrations of the complex at 0.0112 M (cuprous cyanoacetate (0.005 g), tricyclohexylphosphine (0.019 g)); 0.0223 M (cuprous cyanoacetate (0.010 g), tricyclohexylphosphine (0.037 g)); and 0.0446 M (cuprous cyanoacetate (0.02 g), tricyclohexylphosphine (0.076 g)) in an analogous manner as described above.

Note: As the copper concentration increases, the $\nu(CO_2)$ asymmetric stretch at 1635 cm^{-1} shifts to 1639 cm^{-1}, which is indicative of an increased dissociation of the copper carboxylate.

$^{13}CO_2$ Exchange with $[(Ph_3P)_2CuO_2CCH_2CN]_2$ in the Presence of 10 equiv of Triphenylphosphine. $[(Ph_3P)_2CuO_2CCH_2CN]_2$ (0.09 g) and triphenylphosphine (0.18 g) were loaded in a 25 mL flask. DME (3 mL) was cannulated into the above flask, and a $^{13}CO_2$ atmosphere was placed over it. The solution was maintained at 40 °C. The $^{13}CO_2$ exchange rate data were collected by following the disappearance of $\nu(CO_2)$ asymmetric stretch at 1641 cm^{-1} and simultaneous appearance of $\nu(^{13}CO_2)$ infrared band at 1599 cm^{-1}.

$^{13}CO_2$ Exchange with [PPN][O_2CCH_2CN]. In a 25 mL flask was loaded [PPN][O_2CCH_2CN] (0.2 g). Acetonitrile (5 mL) was cannulated into the above flask, and a $^{13}CO_2$ atmosphere was placed over the solution. The solution was maintained at 55.4 °C. The $^{13}CO_2$ exchange rate data were collected by following the disappearance of $\nu(CO_2)$ asymmetric stretch at 1642 cm^{-1} and simultaneous appearance of $\nu(^{13}CO_2)$ infrared band at 1598 cm^{-1}.

$^{13}CO_2$ Exchange with (η^3-HB(Phpz)$_3$)ZnO_2CCH_2CN. In a 25 mL flask (0.2 g) was loaded (η^3-HB(Phpz)$_3$)ZnO_2CCH_2CN. Tetrahydrofuran (5 mL) was cannulated into the above flask, and a $^{13}CO_2$ atmosphere was placed over the solution. The solution was maintained at 55.4 °C. The $^{13}CO_2$ exchange rate data were collected by following the disappearance of $\nu(CO_2)$ asymmetric stretch at 1663 cm^{-1} and simultaneous appearance of $\nu(^{13}CO_2)$ infrared band at 1608 cm^{-1}.

Note: All the rate constants reported herein were calculated from linear plots of ln (absorbance) or absorbance *vs* time, which had correlation coefficients, criteria of the goodness of the linear correlation, in the range 0.961−0.998 (generally above 0.988).

X-ray Crystallographic Study of 3, 4, and 5. Crystal data and details of data collection are given in Table 1. A colorless plate [0.12 mm × 0.24 mm × 0.38 mm] for **3**, a colorless plate [0.10 mm × 0.20 mm × 0.30 mm] for **4**, and a colorless crystal [0.2 mm × 0.2 mm × 0.4 mm] for **5** were mounted on glass fibers, at room temperature. Preliminary examination and data collection were performed on a Rigaku AFC5R X-ray diffractometer (oriented graphite monochromator). Cell parameters were calculated from the least-squares fitting of the setting angles for 25 reflections. ω scans for several intense reflections indicate acceptable crystal quality. Data were collected for $5.0° \le 2\theta \le 120.0°$ for **3** and **4**, and $5.0° \le 2\theta \le 50°$ for **5** at 293 K. For **3**, **4**, and **5**, three control reflections, collected every 150 reflections, showed no significant trends. Background measurements were taken by stationary crystal and stationary counter techniques at the beginning and end of each scan for 0.50 of the total scan time. Lorentz and polarization corrections applied to 6467 reflections for **3**, 6326 reflections for **4**, and 10 572 reflections for **5**. A semiempirical absorption correction was applied. A total of 2807 unique reflections ($R_{int} = 0.05$), with $|I| \ge 2.0\sigma I$ for **3**, 4865 unique reflections ($R_{int} = 0.03$) for **4**, and 10 140 unique reflections ($R_{int} = 0.0253$) for **5** were used in further calculations. The structures were solved by Direct Methods [SHELXS, SHELXTL-PLUS program package, Sheldrick (1990) for **3** and **4**, and SHELXS 1993 for **5**]. Full-matrix least-squares anisotropic refinement for all non-hydrogen atoms in **3** yielded $R = 0.064$, $R_w = 0.061$ and $S = 1.45$, in **4** provided $R = 0.0491$, $R_w = 0.0609$, and $S = 1.95$, and in **5** provided $R = 0.0472$, $R_w^2[I > 2\sigma(I)] = 0.0995$, and $S = 1.010$ at convergence. Hydrogen atoms were placed in idealized positions with isotropic thermal parameters fixed at 0.08 $Å^2$. Neutral atom scattering factors and anomalous-scattering correction terms were taken from *International Tables for X-ray Crystallography*.

The following atoms in complex **4** were disordered over two positions: C3, C3′; C4, C4′; C5, C5′; C6, C6′; C7, C7′; C8, C8′. The atoms C2 and C3, C3 and C4, C2 and C3′, and C3′ and C4′ were fixed at a distance of 1.54(1) Å and allowed to refine. The atoms C2 and C4, and C2 and C4′ were fixed at a distance of 2.48(1) Å and allowed to refine. Atoms C3, C4, C5′, C6′, C7′, and C8′ were located with 30% partial occupancy. Atoms C3′, C4′, C5, C6, C7, and C8 were located with 70% partial occupancy.

Table 1. Crystallographic Data and Data Collection Parameters

	3	**4**	**5**
formula	$C_{78}H_{136}O_4P_4N_2Cu_2$	$C_{40}H_{72}O_2P_2Cu$	$C_{60}H_{48}B_2N_{14}O_4Zn_2$
formula weight	1416.8	710.5	1181.48
space group	monoclinic, $P2_1/n$	triclinic, $P\bar{1}$	triclinic, $P\bar{1}$
a (Å)	10.619(2)	9.706(2)	13.197(2)
b (Å)	20.628(3)	10.442(2)	14.657(2)
c (Å)	18.146(3)	22.423(4)	16.049(3)
α (deg)		97.51(2)	103.44(1)
β (deg)	93.89(1)	92.30(2)	107.10(1)
γ (deg)		116.22(1)	92.19(1)
V ($Å^3$)	3965.9(11)	2008.9(8)	2866.8(8)
Z	2	2	2
density (calcd) (g/cm^3)	1.186	1.174	1.369
absorption coeff (mm^{-1})	1.762	1.731	0.897
λ (Å)	1.54178	1.54178	0.71073
T (K)	293	293	293(2)
transmission coeff	0.8887−0.9999	0.9000−0.9999	
R^a (%)	6.40	4.91	4.72
$R_w{}^a$ (%)	6.10	6.09	9.95[b]

[a] $R = \sum|F_o - F_c|/\sum F_o$. $R_w = \{[\sum w(F_o - F_c)^2]/[\sum w(F_o)^2]\}^{1/2}$. GOF = 1.37, 1.95, and 1.01 for complexes **3**, **4**, and **5**, respectively. [b] $R_w = \{[\sum w(F_o^2 - F_c^2)^2]/[\sum w(F_o^2)^2]\}^{1/2}$.

Results

Synthesis of Copper(I) Derivatives and Their Solution and Solid-State Structures. The dimeric complex of copper(I), $[(Ph_3P)_2CuO_2CCH_2CN]_2$ (**1**), was synthesized as a white powder

Table 2. Summary of Bond Distances and Bond Angles in Complexes **1a**, **1b**, and **2** and Free Cyanoacetic Acid

bonding parameters (average values)	complex			free acid[d]
	1a[a]	**1b**[b]	**2**[c]	
Cu–P (Å)	2.261(2)	2.263(1)	2.264(2)	
Cu–N (Å)	2.061(3)	2.128(3)	2.083(4)	
Cu–O (Å)	2.078(3)	2.074(3)		
C–C[e] (Å)	1.570(7)	1.560(6)	1.526(8)	1.497(4)
C≡N (Å)	1.130(5)	1.125(5)	1.135(6)	1.117(4)
P–Cu–P (deg)	122.1(1)	125.1(1)	123.1(1)	
N–Cu–N (deg)			86.2(2)	
O–Cu–N (deg)	91.3(1)	88.2(1)		

[a] Taken from ref 2c. [b] Taken from ref 11. [c] Taken from ref 10. [d] Kanters, G. R.; Straver, L. H. *Acta Crystallogr.* **1978**, *B34*, 1393. Kanters, G. R.; Roelofsen, G.; Straver, L. H. *Acta Crystallogr.* **1978**, *B34*, 1396. [e] Refers to the C–CO_2 bond.

from the reaction of copper(I) *n*-butyrate and 1 equiv of $NCCH_2COOH$ and 2 equiv of PPh_3 in diethyl ether at ambient temperature. Recrystallization of **1** from a dichloromethane solution layered with diethyl ether maintained at −20 °C resulted in X-ray quality crystals of **1** solvated with Et_2O (**1a**). The infrared spectrum of **1** in DME revealed the cyanoacetate ligand to be monodentate coordinated *via* the carboxylate group ($\nu(CO_2)$ 1609 and 1372 cm^{-1}),[7] which was verified by $^{13}CO_2$ labeling[8] and N-bound through the cyano linkage ($\nu(C{\equiv}N)$ 2255 cm^{-1}).[9] Importantly, this mode of cyanoacetate binding persists in the solid state, as confirmed by observations of the $\nu(CO_2)$ asymmetric and symmetric stretches at 1609 and 1373 cm^{-1} and the $\nu(CN)$ at 2255 cm^{-1} in KBr.

A monoprotonated version of complex **1**, the monomeric complex $(Ph_3P)_2Cu(O_2CCH_2CN)_2H$ (**2**), has previously been crystallized from the reaction of $CH_3Cu(PPh_3)_3$ and 2 equiv of cyanoacetic acid.[10] Interestingly, complex **2** is unstable in solution with respect to dimer formation, *i.e.*, upon dissolution of complex **2** in THF, quantitative formation of complex **1** and 2 equiv of cyanoacetic acid occurs (eq 5). Furthermore, attempts

$$2(Ph_3P)_2Cu(O_2CCH_2CN)_2H \overset{THF}{\rightleftharpoons} [(PPh_3P)_2Cu(O_2CCH_2CN)]_2 + 2NCCH_2COOH \quad (5)$$

to crystallize complex **2** from a THF solution of **1** in the presence of 2 equiv of cyanoacetic acid layered with hexane at −20 °C only provided crystals of **1** solvated by THF (**1b**) as confirmed by X-ray crystallography.[11] Nevertheless, in the presence of large excesses of cyanoacetic acid, complex **1** is in part converted into an alternative copper(I) species, presumably complex **2**, which is less active as a decarboxylation catalyst (*vide infra*). Although the solid-state structures of complexes **1a**, **1b**, and **2** have been briefly described elsewhere, it is worthwhile to summarize crystallographic data pertinent to future discussions at this time in Table 2. In addition, some of the corresponding bonding parameters in free cyanoacetic acid are listed in Table 2.

On the basis of previous observations,[12] it is anticipated that upon employing sterically encumbering ligands,[13,14] such as tricyclohexylphosphine (170°) or tri-*o*-tolylphosphine (194°) *in lieu* of triphenylphosphine (145°), in the analogous synthesis of **1** would result in formation of monomeric copper(I) derivatives. Indeed, the complex prepared from tricyclohexylphosphine, $(Cy_3P)_2CuO_2CCH_2CN$ (**3**), has been shown to be monomeric in the solid state. Single X-ray quality crystals were obtained from a concentrated hexane/ether solution maintained at −20 °C for several days. Figure 1 shows an ORTEP drawing of the molecule, and selected bond distances and angles are provided in Table 3.

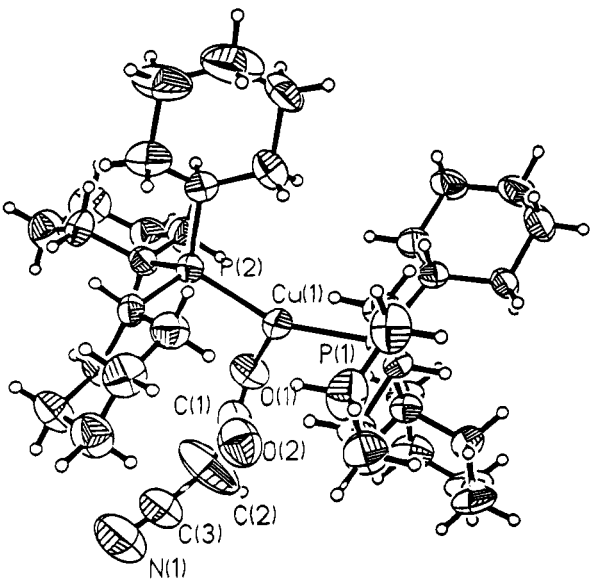

Figure 1. ORTEP drawing of **3** showing the atom numbering scheme. Thermal ellipsoids are drawn at the 50% probability level.

Table 3. Selected Bond Lengths (Å)[a] and Bond Angles (deg) for **3**

Cu(1)–P(1)	2.229(2)	Cu(1)–P(2)	2.243(3)
Cu(1)–O(1)	2.119(7)	P(1)–C(9)	1.849(8)
P(1)–C(15)	1.851(8)	P(1)–C(21)	1.850(8)
P(2)–C(27)	1.870(9)	P(2)–C(33)	1.844(8)
P(2)–C(39)	1.861(8)	O(1)–C(1)	1.23
O(2)–C(1)	1.21	N(1)–C(3)	1.10
C(3)–C(2)	1.38	C(2)–C(1)	1.52
P(1)–Cu(1)–P(2)	145.2(1)	P(1)–Cu(1)–O(1)	111.7(2)
P(2)–Cu(1)–O(1)	102.8(2)	Cu(1)–P(1)–C(9)	110.7(3)
Cu(1)–P(1)–C(15)	113.5(3)	Cu(1)–P(2)–C(27)	119.0(3)
Cu(1)–P(1)–C(21)	114.8(3)	Cu(1)–O(1)–C(1)	101.7(7)
Cu(1)–P(2)–C(33)	111.0(3)	C(3)–C(2)–C(1)	119
Cu(1)–P(2)–C(39)	109.3(3)	O(1)–C(1)–C(2)	117
N(1)–C(3)–C(2)	176		
O(1)–C(1)–O(2)	127		
O(2)–C(1)–C(2)	116		

[a] Estimated standard deviations are given in parentheses.

Complex **3** displays a distorted trigonal planar geometry and is structurally analogous to the previously reported bis(triphenylphosphine)cuprous hydrogen malonate.[15] The large distortion from an ideal trigonal planar geometry results from the extreme steric crowding of the two tricyclohexylphosphine ligands, which results in a P–Cu–P bond angle of 145.2(1)°. For comparison, the P–Cu–P bond angle in the $(Ph_3P)_2CuO_2CH_2CO_2H$ derivative is 131.1°.[15] The cyanoacetate ligand is bound in a monodentate fashion through the carboxylate functionality with a Cu–O(1) bond distance of 2.119(7) Å. The Cu–O(2) distance of 2.632 Å is indicative of no interaction. Earlier reports on bis(phosphine)cuprous carboxylates have

(7) Nakamoto, K. *Infrared and Raman Spectra of Inorganic and Coordination Compounds*, 4th ed.; Wiley: New York, 1986; pp 231–233. $\Delta = \nu(CO_2)asym - \nu(CO_2)sym = 241\ cm^{-1}$, which is much greater than the difference observed in free cyanoacetate ion ($\Delta = 200\ cm^{-1}$), thus supporting a unidentate mode of coordination.

(8) The corresponding $\nu(^{13}CO_2)$ data in DME were observed at 1560 and 1347 cm^{-1} for the asymmetric and symmetric stretches, respectively.

(9) Purcell, K. F.; Drago, R. S. *J. Am. Chem. Soc.* **1966**, *88*, 919.

(10) Darensbourg, D. J.; Longridge, E. M.; Atnip, E. V.; Reibenspies, J. H. *Inorg. Chem.* **1991**, *30*, 357.

(11) Reibenspies, J. H.; Darensbourg, D. J.; Niezgoda, S. A.; Holtcamp, M. H.; Klausmeyer, K. K. *Z. Kristallogr.* **1994**, *209*, 552.

(12) Darensbourg, D. J.; Holtcamp, M. W.; Khandelwal, B.; Klausmeyer, K. K.; Reibenspies, J. H. *Inorg. Chem.* **1994**, *33*, 2036.

(13) Tolman, C. A. *Chem. Rev.* **1977**, *77*, 313.

(14) Brown, T. L. *Inorg. Chem.* **1992**, *31*, 1286.

Table 4. Bond Lengths (Å)[a] and Bond Angles (deg) for **4**

Cu(1)−P(1)	2.231(1)	Cu(1)−P(2)	2.248(1)
Cu(1)−O(1)	2.276(4)	Cu(1)−O(2)	2.181(3)
Cu(1)−C(1)	2.550(5)	O(1)−C(1)	1.233(7)
O(2)−C(1)	1.232(8)	O(1)−C(2)	1.508(9)
C(2)−C(3)	1.49(2)	C(2)−C(3)	1.52(2)
C(3)−C(4)	1.56(1)	C(3)′−C(4)′	1.53(2)
P(1)−Cu(1)−P(2)	137.4(1)	P(1)−Cu(1)−O(1)	109.7(1)
P(2)−Cu(1)−O(1)	102.3(1)	P(1)−Cu(1)−O(2)	111.3(1)
P(2)−Cu(1)−O(2)	109.4(1)	P(1)−Cu(1)−C(1)	114.4(1)
P(2)−Cu(1)−C(1)	107.3(1)	Cu(1)−P(1)−C(10)	113.1(2)
Cu(1)−P(1)−C(16)	109.9(1)	C(10)−P(1)−C(16)	108.4(2)
Cu(1)−P(1)−C(22)	117.4(1)	C(10)−P(1)−C(22)	103.9(2)
C(16)−P(1)−C(22)	103.4(2)	Cu(1)−P(2)−C(28)	115.9(1)
Cu(1)−P(2)−C(34)	112.3(1)	C(28)−P(2)−C(34)	102.9(2)
Cu(1)−P(2)−C(40)	110.6(1)	C(28)−P(2)−C(40)	110.5(2)
C(34)−P(2)−C(40)	103.8(2)	Cu(1)−O(1)−C(1)	88.0(3)
Cu(1)−O(2)−C(1)	92.5(3)	Cu(1)−C(1)−O(1)	63.1(3)
O(1)−C(1)−O(2)	121.7(5)	Cu(1)−C(1)−C(2)	177.4(4)
O(1)−C(1)−C(2)	119.2(6)	O(2)−C(1)−C(2)	119.0(5)

[a] Estimated standard deviations are given in parentheses.

shown that an interaction of the distal carboxylate's oxygen atom distorts the copper(I) center toward tetrahedral geometry.[15] Consistent with the lack of Cu···O(2) bonding, no such distortion is evident in complex **3** as seen by the very small deviation from planarity (0.0259 Å). The most significant comparison between the dimer (complex **1**) and the monomer (complex **3**) is seen in the C−C bond distance in the O_2C−CH_2CN ligand. Complex **3** has a C(1)−C(2) bond distance of 1.52(2) Å, whereas in complex **1**, the corresponding bond distance is 1.570(7) Å. This elongation of the C(1)−C(2) bond distance in **1** is the result of the cyano moiety coordinating to the copper(I) center, where electron density is shifted away from the carboxylate functionality.

As in the case of complex **1**, complex **3** has a monodentate-coordinated carboxylate group in THF solution, as well as in the solid state, as indicated by $\nu(CO_2)_{asym}$ and $\nu(CO_2)_{sym}$ being observed at 1635 and 1339 cm^{-1} (Δ = 296 cm^{-1}), and 1628 and 1354 cm^{-1} (Δ = 274 cm^{-1}) in KBr, respectively. The monodentate behavior exhibited by the cyanoacetate ligand toward copper(I) is typical for carboxylates with electron-withdrawing substituents.[16] However, in this instance, steric interactions may also play a role in determining whether the carboxylate is chelated or monodentate. In order to differentiate between steric and electronic contributions of the phosphine and carboxylate ligands, respectively, on the nature of the cyanoacetate binding to copper(I), we have synthesized and characterized by X-ray crystallography the $(Cy_3P)_2Cu(O_2CCH_2CH_2CH_3)$ (**4**) derivative. Complexes **3** and **4** allow for a convenient comparison of two $(Cy_3P)_2Cu$(carboxylate) derivatives in which the carboxylates are approximately the same size but differ significantly in basicity (pK_a of cyanoacetic acid = 2.85 and pK_a of butyric acid = 4.81).[17]

Colorless crystals of complex **4** were obtained from a hexane/diethyl ether solution maintained at −20 °C. Selected interatomic distances and angles for complex **4** are provided in Table 4. Figure 2 illustrates the perspective drawing of complex **4** with the atomic numbering scheme. The more basic butyrate ligand is found asymmetrically chelated to the $(Cy_3P)_2Cu(I)$ moiety.[18] The Cu(1)−O(1) and Cu(1)−O(2) bond distances are 2.276(5) and 2.182(4) Å, respectively. The interaction of O(1)

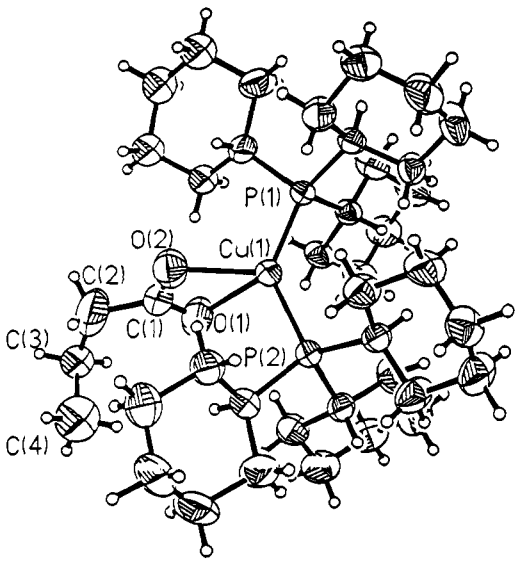

Figure 2. ORTEP drawing of **4** showing the atom numbering scheme. Thermal ellispoids are drawn at the 50% probability level.

distorts the trigonal planar geometry that exists for bis(phosphino)copper(I) nonchelated carboxylates (planar deviation = 0.0655 Å). A severely distorted tetrahedral geometry results. The P(1)−Cu(1)−P(2) bond angle is 137.5(1)°, and the Cu(1)−P(1) and Cu(1)−P(2) bond distances are 2.232(1) and 2.248(1) Å, respectively. At least in these examples we can conclude that steric interactions do not determine whether the carboxylate ligand coordinates monodentate or bidentate. A comparison of these two structures implies that electronic effects control the coordination motif of the carboxylate.

Synthesis of (η^3-HB(3-Phpz)$_3$)$ZnO_2CCH_2CN\cdot 2H_2O$ (5) and Its Solid-State Structure. In order to compare reactivity patterns with regard to decarboxylation processes between copper(I) and zinc(II), we have synthesized the cyanoacetate derivative of zinc(II) hydrotris(3-phenylpyrazoyl)borate. Complex **5** was prepared from the reaction of the corresponding acetate derivative,[19] (η^3-HB(3Phpz)$_3$)ZnO_2CCH_3, and cyanoacetic acid in tetrahydrofuran. The infrared spectrum of **5** in THF indicated a nonbonded −CN linkage (2262 cm^{-1}) and an asymmetric $\nu(CO_2)$ vibration split at 1662 and 1651 cm^{-1}, indicative of monodentate binding. Similar vibrational modes were evident in the solid state at 2264, 1662, and 1649 cm^{-1} as determined in KBr.

Crystals of **5** suitable for X-ray analysis were obtained by the slow diffusion of diethyl ether into a concentrated dichloromethane solution of the complex. Selected interatomic bond distances and bond angles for complex **5** are provided in Table 5. Complex **5** displays a distorted tetrahedral geometry in which two crystallographically distinct molecules cocrystallized. An ORTEP drawing of one of the molecules, along with the atom numbering scheme, may be found in Figure 3. The major differences between the two molecules are seen in the Zn−O bond distances (Zn(1)−O(1) = 1.908(2) Å, Zn(1)−O(2) = 2.660 Å, Zn(2)−O(3) = 1.917(3) Å, Zn(2)−O(4) = 2.581 Å). The Zn−N bond distances are very similar with the average Zn(1)−N bond distance = 2.036 Å and the average Zn(2)−N bond distance = 2.038 Å. The other major difference was found in

(15) Darensbourg, D. J.; Holtcamp, M. W.; Khandelwal, B.; Reibenspies, J. H. *Inorg. Chem.* **1994**, *33*, 531.
(16) Hammond, B.; Jardine, F. H.; Vohra, A. G. *J. Inorg. Nucl. Chem.* **1971**, *33*, 1017.
(17) *Handbook of Chemistry and Physics*, 70th ed.; Weast, R. C., Ed.; CRC Press, Inc.: Boca Raton, FL, D-163, 1990.
(18) Darensbourg, D. J.; Holtcamp, M. W.; Longridge, E. M.; Klausmeyer, K. K.; Reibenspies, J. H. *Inorg. Chim. Acta* **1994**, *227*, 223.
(19) The corresponding synthesis of (hydrotris(3-*tert*-butylpyrazoyl)borate)$Zn(O_2CCH_3)$ has been reported in ref 20, along with its X-ray structure.
(20) Han, R.; Gorell, I. B.; Looney, A. G.; Parkin, G. *J. Chem. Soc., Chem. Commun.* **1991**, 717.

Table 5. Selected Bond Lengths (Å)[a] and Bond Angles (deg) for **5**

Zn(1)–O(1)	1.908(2)	Zn(1)–N(7)	2.019(3)
Zn(1)–N(2)	2.024(3)	Zn(1)–N(5)	2.066(3)
Zn(2)–N(9)	2.018(3)	Zn(2)–O(3)	1.917(3)
Zn(2)–N(13)	2.073(3)	Zn(2)–N(11)	2.024(3)
O(1)–C(1)	1.280(5)	O(2)–C(1)	1.208(5)
O(3)–C(31)	1.285(5)	O(4)–C(31)	1.204(5)
N(1)–C(3)	1.107(6)	N(8)–C(33)	1.110(6)
C(1)–C(2)	1.507(6)	C(2)–C(3)	1.451(6)
C(32)–C(33)	1.442(6)	C(31)–C(32)	1.523(6)
O(1)–Zn(1)–N(7)	123.46(13)	O(1)–Zn(1)–N(2)	124.94(13)
N(7)–Zn(1)–N(2)	97.76(13)	O(1)–Zn(1)–N(5)	118.17(12)
N(7)–Zn(1)–N(5)	93.84(13)	N(2)–Zn(1)–N(5)	90.24(13)
O(3)–Zn(2)–N(9)	124.13(13)	O(3)–Zn(2)–N(11)	124.92(13)
N(9)–Zn(2)–N(11)	98.00(14)	O(3)–Zn(2)–N(13)	118.38(14)
N(9)–Zn(2)–N(13)	91.05(13)	N(11)–Zn(2)–N(13)	91.39(14)
O(2)–C(1)–O(1)	125.3(4)	O(2)–C(1)–C(2)	122.0(4)
O(1)–C(1)–C(2)	112.7(4)	O(2)–C(1)–Zn(1)	80.3(2)
O(1)–C(1)–Zn(1)	45.1(2)	C(2)–C(1)–Zn(1)	157.6(3)
C(3)–C(2)–C(1)	114.3(4)	N(1)–C(3)–C(2)	176.7(6)
C(29)–C(30)–C(24)	118.5(4)	C(4)–C(5)–C(6)	105.9(4)
O(4)–C(31)–C(32)	122.1(4)	O(4)–C(31)–O(3)	125.4(4)
O(4)–C(31)–Zn(2)	78.2(2)	O(3)–C(31)–C(32)	112.6(4)
C(32)–C(31)–Zn(2)	159.7(3)	O(3)–C(31)–Zn(2)	47.2(2)
N(8)–C(33)–C(32)	178.4(6)	C(33)–C(32)–C(31)	112.6(4)

[a] Estimated standard deviations are given in parentheses.

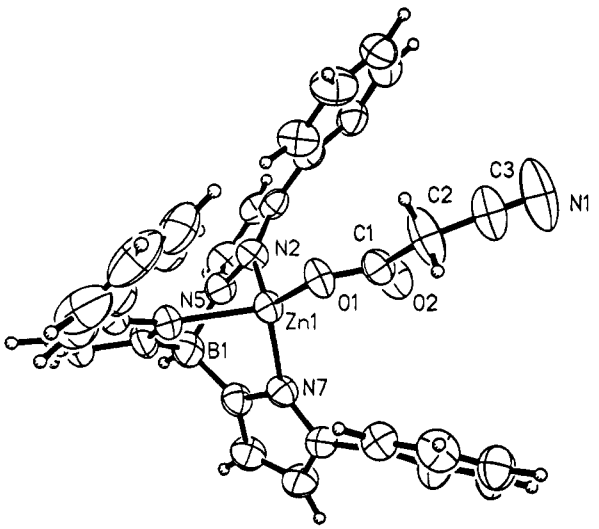

Figure 3. ORTEP drawing of one of the two crystallographic independent molecules of **5** showing the atom numbering scheme. Thermal ellipsoids are drawn at the 50% probability level.

the O(1)–Zn(1)–N(7) and O(3)–Zn(2)–N(9) bond angles of 123.46(13)° and 124.13(13)°, respectively. Complex **5** is structurally quite similar to (hydrotris(3-*tert*-butylpyrazolyl)-borate)zinc nitrate[21] and (hydrotris(3-phenylpyrazolyl)borate)-zinc nitrate[22] in which highly asymmetric Zn–O bonds are present.

Decarboxylation of Cyanoacetic Acid Mediated by Copper(I) and Zinc(II) Complexes. The central step in the metal-catalyzed decarboxylation of cyanoacetic acid is the extrusion of CO_2 from the metal-bound carboxylate (reverse reaction in eq 1). As mentioned previously, in group 6 metal chemistry this reaction does not occur, although the metal carboxylate is very active as a catalyst precursor for cyanoacetic acid decomposition to acetonitrile and CO_2.[4] On the other hand, in the case of copper(I) chemistry, both CO_2 extrusion from copper(I) cyanoacetate and decarboxylation of cyanoacetic acid

(21) Han, R.; Parkin, G. *J. Am. Chem. Soc.* **1991**, *113*, 9707.
(22) Alsfasser, R.; Powell, A. K.; Vahrenkamp, H. *Angew. Chem., Int. Ed. Engl.* **1990**, *29*, 898.

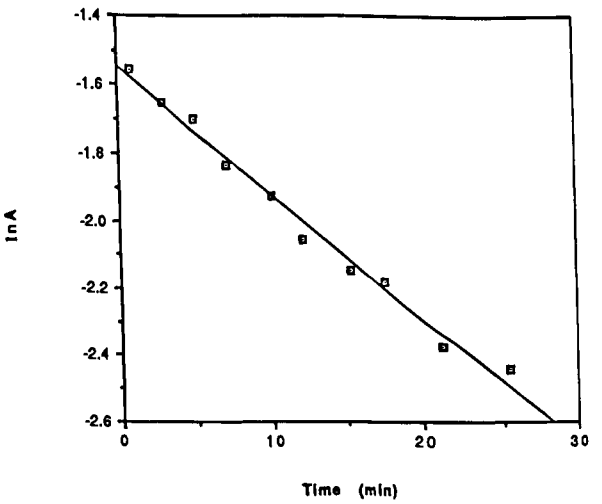

Figure 4. First-order plot of rate data for the exchange reaction of complex **1** with $^{13}CO_2$ at 40.0 °C in DME.

Table 6. Rate Constants as a Function of Temperature: (i) Catalytic Decarboxylation of Cyanoacetic Acid in Presence of **1** and (ii) $^{13}CO_2$ Exchange in **1**[a]

T (K)	(i) 10^3k_{obs} (s^{-1})[b]	(ii) 10^3k_{obs} (s^{-1})[c]
297.9	0.144	0.224
302.9		0.234
308.0	0.402	0.456
313.0	0.863	0.690
318.0	1.59	1.12
323.0	3.06	2.33

[a] Reactions were carried out in DME solutions. The concentration of catalyst in (i) was 0.004 M and the concentration of acid was 0.0225 M. [b] $\Delta H^{\ddagger} = 23.5 \pm 1.2$ kcal mol^{-1} and $\Delta S^{\ddagger} = 0.41 \pm 3.9$ eu; at 298 K $\Delta G^{\ddagger} = 23.4$ kcal mol^{-1}. [c] $\Delta H^{\ddagger} = 18.2 \pm 1.9$ kcal mol^{-1} and $\Delta S^{\ddagger} = -10.6 \pm 6.1$ eu; at 298 K $\Delta G^{\ddagger} = 21.4$ kcal mol^{-1}.

in the presence of copper(I) cyanoacetate to yield CO_2 and CH_3CN exclusively readily occur. In the former process the reaction is reversible and can be studied employing $^{13}CO_2$ as a probe as depicted in the skeletal eq 6. In this instance the mechanistic

$$MO_2CCH_2CN + {}^{13}CO_2 \rightleftharpoons MO_2{}^{13}CCH_2CN + CO_2 \quad (6)$$

aspects of the CO_2 extrusion and reinsertion can be examined in the absence of added cyanoacetic acid.

Complex **1**, $[(Ph_3P)_2CuO_2CCH_2CN]_2$, was found to easily undergo CO_2 exchange in DME over the temperature range of 25–50 °C. The exchange process was monitored in the presence of a large excess of $^{13}CO_2$ by observing the decrease in absorbance of the asymmetric $\nu(CO_2)$ stretching frequencies in **1** at 1609 cm^{-1}. The $^{13}CO_2$ exchange at the carboxylate site was noted by the appearance of the corresponding asymmetric $\nu(^{13}CO_2)$ vibrational mode at 1560 cm^{-1} in the infrared, as well as a ^{13}C NMR signal at 167.4 ppm. Concomitantly, during the progress of the exchange process, there was an increase in the free $^{12}CO_2$ in solution (2338 cm^{-1}) relative to dissolved $^{13}CO_2$ (2272 cm^{-1}). The $^{13}CO_2$ exchange in complex **1** occurred *via* a first-order process as seen by the linear plot of ln (absorbance) *vs* time in Figure 4. The first-order rate constants for CO_2 exchange in complex **1** were measured as a function of temperature, and these data are compiled in Table 6, along with the derived activation parameters.

In like fashion, the monomeric complex **3** containing the tricyclohexylphosphine ligand underwent $^{13}CO_2$ exchange, albeit at a faster rate. The rate of the exchange reaction was measured by observing the disappearance of the asymmetric carboxylate

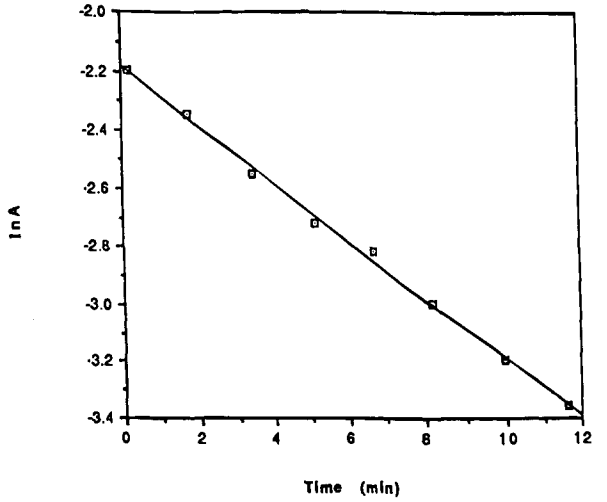

Figure 5. First-order plot of rate data for the exchange reaction of complex **3** with $^{13}CO_2$ at 20.0 °C in THF.

Table 7. Rate Constants as a Function of Concentration for the $^{13}CO_2$ Exchange of $(Cy_3P)_2Cu(O_2CCH_2CN)$[a]

concentration (M)	10^3k_{obs} (s^{-1})
0.0112	1.3
0.0223	1.2
0.0446	0.62
0.0892	0.57

[a] Reactions were carried out in THF solution at a temperature of 20.0 °C.

stretch (1639−1635 cm^{-1}) in THF, with the concomitant appearance of the corresponding ^{13}C-labeled stretch at 1596−1595 cm^{-1}. The reaction was again first-order in [**3**] as demonstrated by the linear plot depicted in Figure 5. Table 7 contains kinetic data for the exchange process carried out at several different concentrations where only a slight decrease in exchange rate was noted over a greater than 8-fold increase in the [**3**].

As a control experiment we examined the $^{13}CO_2$ exchange reaction involving the free cyanoacetate anion by measuring the rate of ^{13}C-label incorporation into an acetonitrile solution of the $[PPN][NCCH_2CO_2]$ salt. This was accomplished by monitoring the disappearance of the asymmetric $\nu(CO_2)$ vibration at 1642 cm^{-1} while simultaneously following the appearance of the corresponding $\nu(^{13}CO_2)$ vibrational mode at 1598 cm^{-1}. The first-order rate constant, determined in the presence of a large excess of $^{13}CO_2$, was found to be 2.42×10^{-4} s^{-1} at 55.4 °C. This observation clearly indicates the instability of cyanoacetate salts toward decarboxylation, even in the absence of metal interaction. Nevertheless, the rate of CO_2 exchange in this instance is much slower (by a factor of about 0.06) than in the presence of copper(I) complexes. This is proof that the exchange is assisted by copper(I) and is not simply occurring *via* a mechanism involving predissociation of cyanoacetate from the metal with no further association with the copper(I) center.[23]

Indeed, coordination of cyanoacetate *via* the carboxylate functionality to the zinc pyrazolyl hydroborate cation inhibits the CO_2 exchange reaction. That is, the first-order rate constant

(23) This is indeed the case for the decarboxylation of copper(I) derivatives of malonic acid. In this instance, we have found that salts containing noninteracting cations, *e.g.*, $[(C_2H_5)_4N][O_2CCH_2CO_2H]$, are much more effective catalysts for decarboxylation of malonic acid than those of copper(I). Hence, the copper(I) malonate salts simply serve as a source of the malonate anion. D. J. Darensbourg, M. W. Holtcamp, B. Khandelwal, K. K. Klausmeyer, and J. H. Reibenspies, submitted for publication.

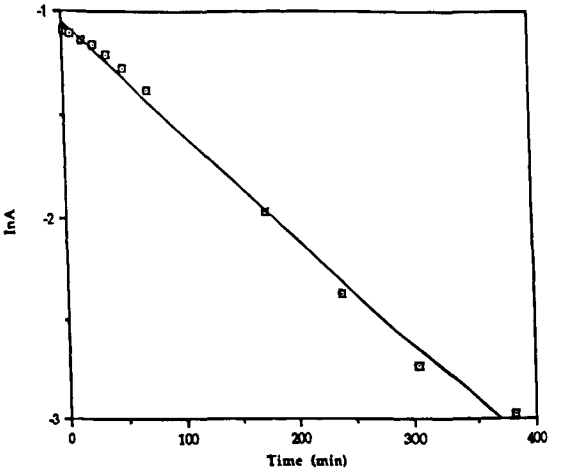

Figure 6. First-order plot of rate data for the exchange reaction of complex **5** with $^{13}CO_2$ at 55.4 °C in THF.

for $^{13}CO_2$ incorporation into (hydrotris(3-phenylpyrazoyl)-borate)ZnO_2CCH_2CN (**5**) in THF was found to be 8.82×10^{-5} s^{-1} at 55.4 °C (Figure 6). During this process the asymmetric $\nu(CO_2)$ stretch at 1663 cm^{-1} shifted to 1608 cm^{-1} upon exchange with ^{13}C-labeled CO_2. (Hydrotris(3-phenylpyrazoyl)-borate)zinc carboxylates are known to form strong Zn−O bonds (1.8−1.9 Å), which are presumably responsible for retarding CO_2 exchange in these zinc(II) derivatives relative to copper(I) ($k_{obs} = 3.55 \times 10^{-3}$ s^{-1} at 55.4 °C in DME). Hence, the cyanoacetate ligand is stabilized toward decarboxylation in the presence of (hydrotris(3-phenylpyrazoyl)borate)Zn^+.

As would be anticipated based on their abilities to undergo the exchange process with $^{13}CO_2$, complexes **1** and **3** are effective catalysts for the decarboxylation of cyanoacetic acid to acetonitrile and CO_2. The decarboxylation of cyanoacetic acid was monitored by observing the disappearance of the $\nu(CO_2)$ stretch at 1748 cm^{-1} in THF for the free acid. CO_2 production is monitored by the appearance of the infrared band at 2338 cm^{-1}, whereas the appearance of acetonitrile is indicated by the $\nu(CN)$ stretch at 2252 cm^{-1}. The dependence of the reaction upon acid concentration was determined to be of zero-order as indicated by the plot of A/A_o *vs* time, where A and A_o are the absorbances of free acid at time = t and time = 0, respectively. Figure 7 displays the typical zero-order plots obtained using complexes **1** and **3** as catalysts. As is readily seen from the plots in Figure 7, $(Cy_3P)_2CuO_2CCH_2CN$ (**3**) decarboxylates cyanoacetic acid with an enhanced rate as compared to $[(Ph_3P)_2CuO_2CCH_2CN]_2$ (**1**). Temperature dependent rate data for the decarboxylation process catalyzed by complex **1** are provided in Table 6, along with the derived activation parameters. Figure 8 shows comparable Eyring plots for $^{13}CO_2$ exchange in **1** *vs* acid decarboxylation in the presence of **1**. The coincidence of the rate constants near ambient temperature appears to be the result of compensating factors, where the slight increase in $\Delta H^{\ddagger}$ for the latter process is almost completely canceled out by the decrease in $T\Delta S^{\ddagger}$.

A more thorough examination of phosphine/phosphite ligand effects on the catalytic decarboxylation reaction (eq 7) is represented in Table 8, where cuprous cyanoacetate in the presence of 2 equiv of phosphine or phosphine ligand is used as catalyst precursor. The rate constants changed only slightly,

$$NCCH_2COOH \xrightarrow{[cat.]} CH_3CN + CO_2 \qquad (7)$$

and a trend upon increasing basicity of the phosphine donor ligand was not entirely observed. It is worthy at this point to

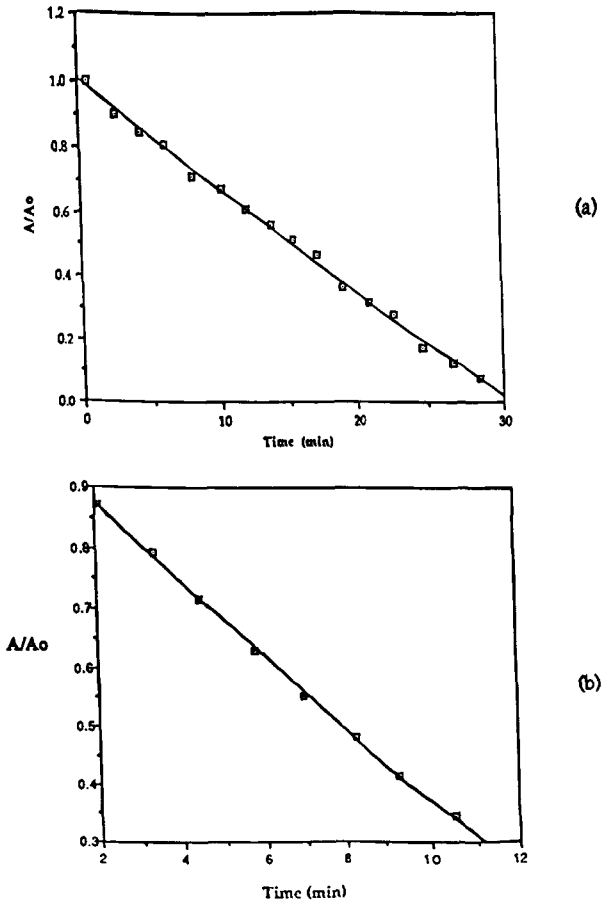

Figure 7. Zero-order plots of rate data for the catalytic decarboxylation of cyanoacetic acid at 40.0 °C in THF in the presence of (a) complex **1** and (b) complex **3**.

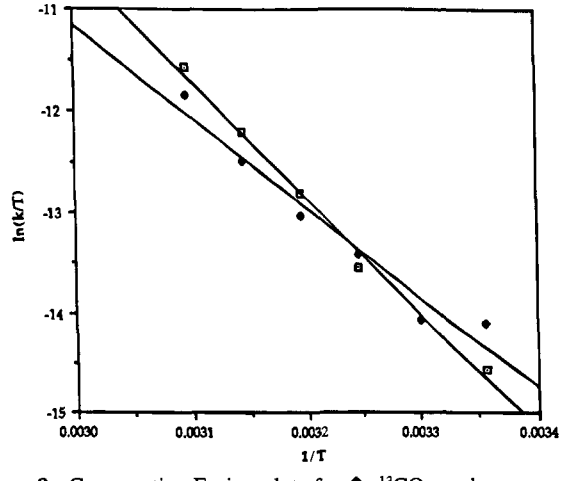

Figure 8. Comparative Eyring plots for ◆, $^{13}CO_2$ exchange reaction with **1**, and ⊡, decarboxylation of cyanoacetic acid in the presence of **1**.

note that slightly enhanced rate constants were observed when the carboxylate functionality was unbound to the metal center during the decarboxylation process as revealed by infrared spectroscopy. For example, triphenylphosphine and tri-*o*-tolylphosphine complexes, which possess carboxylate-bound cyanoacetate ligands, exhibit the lower rate constants for decarboxylation (Table 8). This observation is important in that it lends valuable insight into the decarboxylation mechanism (*vide supra*).

The rate of the metal-catalyzed decarboxylation reaction (eq 7) was measured in THF at 40 °C using cuprous cyanoacetate

Table 8. Rate Constants as a Function of Phosphine for the Catalytic Decarboxylation of Cyanoacetic Acid by (Phosphine)$_2$Cu(O_2CCH_2CN)[a]

complex (Cu(cyanoacetate)/ 2 equiv of phosphine)	cone angle (deg)	pK_a	$\nu(CO_2)$ (cm^{-1})[b]	10^3k_{obs} (s^{-1})
$((PhO)_3P)_2Cu$ cyanoacetate	128	−2.0	1636 sharp	0.4
$((MeO)_3P)_2Cu$ cyanoacetate	107	2.6	1646 broad	2.1
$(Ph_3P)_2Cu$ cyanoacetate	145	2.73	1646−1608 broad	1.3
$((o\text{-}MeC_6H_4)_3P)_2Cu$ cyanoacetate	194	3.08	1637 sharp	1.0
$(Et_3P)_2Cu$ cyanoacetate	132	8.69	1640 broad	2.0
$(Cy_3P)_2Cu$ cyanoacetate	170	9.70	1640−1620 broad	4.1

[a] Reactions were carried out in a THF solution. The concentration of acid was 0.047 M, and the concentration of catalyst was 0.0135 M. The temperature was kept constant at 40.0 °C. [b] Complex in the presence of excess cyanoacetic acid.

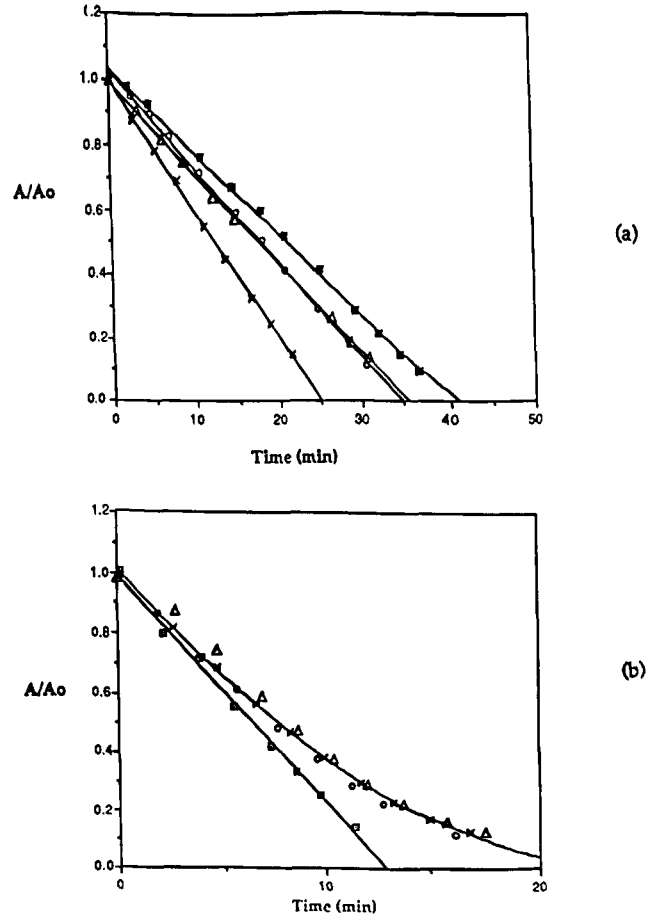

Figure 9. Rate data at 40.0 °C in THF for the catalytic decarboxylation of cyanoacetic acid in the presence of copper(I) cyanoacetate as a function of added phosphine. (a) PPh_3: ■, 2 equiv; ○, 3 equiv; △, 4 equiv; ×, 10 equiv. (b) Cy_3P: ⊡, 2 equiv; ○, 3 equiv; △, 4 equiv; ×, 10 equiv.

as a catalyst in the presence of varying quantities of triphenylphosphine and tricyclohexylphosphine. These results are represented as zero-order rate plots in Figure 9, where excess triphenylphosphine (>2 equiv) is shown to enhance the rate of decarboxylation and excess tricyclohexylphosphine slightly inhibits the decarboxylation process. In addition, the decarboxylation reaction catalyzed by complex **1** is inhibited by high concentrations of cyanoacetic acid. In other words, there is an

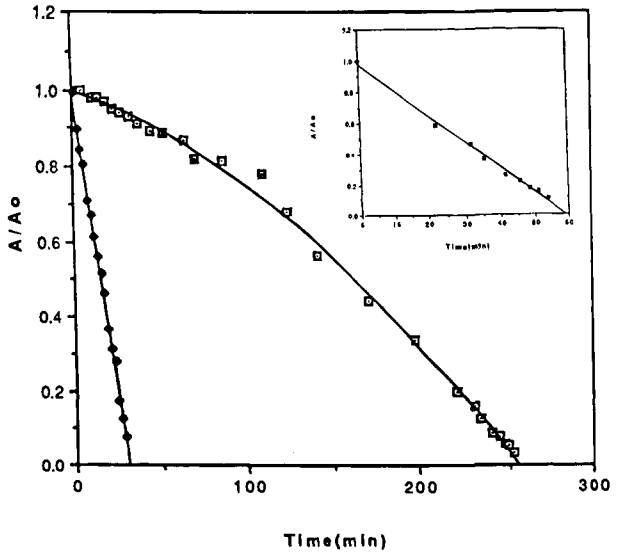

Figure 10. Rate data at 40.0 °C in THF for the catalytic decarboxylation of cyanoacetic acid in the presence of complex **1** as a function of [acid]. (a) ◆, 0.047 M in acid and 0.0135 M in **1**. (b) ⊡, 0.112 M in acid and 0.0185 M in **1**. (Overlay shows zero-order plot obtained for data from the last portion of the reaction where the initial acid concentration has dropped to 0.0370 M.)

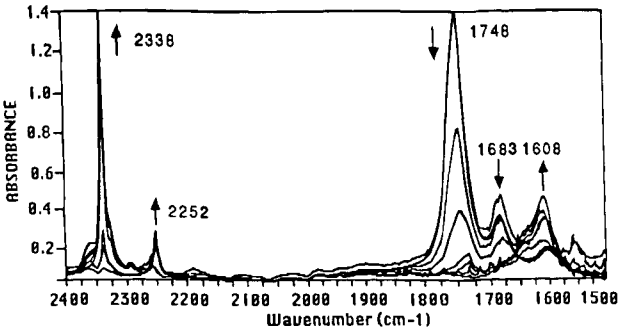

Figure 11. Infrared traces as a function of time for the catalytic decarboxylation of cyanoacetic acid in the presence of complex **1** in the high acid concentration (0.200 M) region.

acid concentration regime where the rate constant is independent of [acid], providing a linear plot of [acid] *vs* time, as well as an acid concentration region where a plot of [acid] *vs* time is nonlinear. For example, Figure 10 displays comparable zero-order plots for two different acid concentrations, 0.047 and 0.112 M, respectively. As is readily observable, the rate of catalytic decarboxylation in the presence of the higher acid concentration is accelerated as the cyanoacetic acid is consumed. Indeed, if the last series of data points in the higher concentration of acid run are considered, where the [acid] has dropped below 0.047 M, the rate constants for decarboxylation in the two instances do not differ greatly (1.3×10^{-3} *vs* 0.58×10^{-3} s^{-1}). The slightly lower rate observed in Figure 10b is largely due to inhibition by the excess of CH_3CN, which has accumulated in solution.[24]

Figure 11 displays the infrared spectra taken during the decarboxylation of cyanoacetic acid catalyzed by complex **1** under conditions where the acid concentration is in the high concentration regime (0.200 M). In addition to the carboxylate-stretching vibration for free cyanoacetic acid at 1748 cm^{-1}, a carboxylate peak at 1683 cm^{-1} is noted. As the cyanoacetic acid concentration decreases, this latter peak decreases with a subsequent increase in the asymmetric $\nu(CO_2)$ mode due to complex **1** at 1608 cm^{-1}. Hence, cyanoacetic acid in high concentrations apparently hydrogen bonds with the active catalyst, forming a new species with $\nu(CO_2)$ at 1683 cm^{-1}. As the concentration of acid decreases due to decarboxylation, the hydrogen-bonded species disappears with concomitant formation of complex **1**. Consistent with the above observations, protonation of the carboxylate ligand in complex **1** with a strong acid, HBF_4, greatly inhibits the rate of decarboxylation. For example, adding 1 equiv of HBF_4 per copper(I) cyanoacetate group in complex **1** leads to a carboxylate stretching frequency at 1744 cm^{-1}, which is very close to that observed for the free acid and completely shuts down the decarboxylation process. That is, only a slight quantity of CO_2 was observed after heating the solution for over 12 h at 40 °C.

Table 9. Rate Constants as a Function of Catalyst for the Catalytic Decarboxylation of Cyanoacetic Acid at 55.4 °C

catalyst	$10^3 k_{obs}$ (s^{-1})	solvent
(TPPZ)Zn(O_2CCH_2CN)[a]	0.07	THF
[(TCDD)Zn(O_2CCH_3)][Ph_4B][b]	0.18	THF
[PPN][O_2CCH_2CN]	0.014	THF
(1,10-Phen)Cu(O_2CCH_3)	10.5[c]	DME
[(Ph_3P)$_2$Cu(O_2CCH_2CN)]$_2$	5.5	DME
[PPN][W(CO)$_5$$O_2CCH_2CN$]	0.033	DME

[a] TPPZ = tris(3-phenylpyrazolyl)hydroborate. [b] TCDD = 1,5,9-triazacyclododecane. [c] 1,10-Phen = 1,10-phenanthroline.

(Hydrotris(3-phenylpyrazoyl)borate)Zn(O_2CCH_2CN) also serves as a catalyst for the decarboxylation of cyanoacetic acid, albeit less effectively than the copper(I) derivatives, with a k_{obs} at 55.4 °C of 7.0×10^{-5} s^{-1}. Nevertheless, this rate of decarboxylation is enhanced over that noted in the presence of [PPN][O_2CCH_2-CN], where k_{obs} was determined to be 1.4×10^{-5} s^{-1} at 55.4 °C. On the other hand, [(1,5,9-triazacyclododecane)Zn(O_2-CCH_3)][BPh_4] is a more active catalyst for the decarboxylation of cyanoacetic acid, providing a k_{obs} of 1.8×10^{-4} s^{-1} at 55.4 °C. Table 9 summarizes the k_{obs} at a common temperature for the various catalysts that have been found active for the decarboxylation of cyanoacetic acid.

Discussion

An inherent difficulty in proposing an explicit mechanistic pathway for the catalytic decarboxylation of cyanoacetic acid in the presence of copper(I) carboxylates stems from the kinetic lability exhibited by copper(I) derivatives. This kinetic lability associated with d^{10} centers makes possible a wider range of copper(I) species that can exist in solution through phosphine dissociation and/or carboxylate dissociation. For example, rapid phosphine exchange has been shown to occur in several copper(I) systems.[25] Nevertheless, based on our observations of kinetic parameters associated with CO_2 exchange in copper(I) carboxylates, coupled with those for acid decarboxylation, we can make some very definitive statements about the salient mechanistic features of metal-catalyzed decarboxylation processes. Scheme 1 represents an outline of our view of this catalytic process.

It is important to note that it is not necessary for the copper(I) complexes in Scheme 1 to be four-coordinate. Indeed, stable copper(I) complexes are commonly isolated with coordination numbers of 2, 3, or 4. Ligand steric requirements most often determine the coordination number of copper(I). For example, bis(tricyclohexylphosphine)copper(I) cyanoacetate is three-

(24) We have previously demonstrated that acetonitrile is an effective inhibitor for the decarboxylation of cyanoacetic acid catalyzed by copper(I). It binds to the copper(I) center, hence, blocking the site for cyanoacetate binding.[3g]

(25) See, for example: (a) Dempsey, D. F.; Girolami, G. S. *Organometallics* **1988**, *7*, 1208. (b) Coan, P. S.; Folting, K.; Huffman, J. C.; Caulton, K. G. *Organometallics* **1989**, *8*, 2724. (c) Darensbourg, D. J.; Holtcamp, M. W. Unpublished observations.

Scheme 1

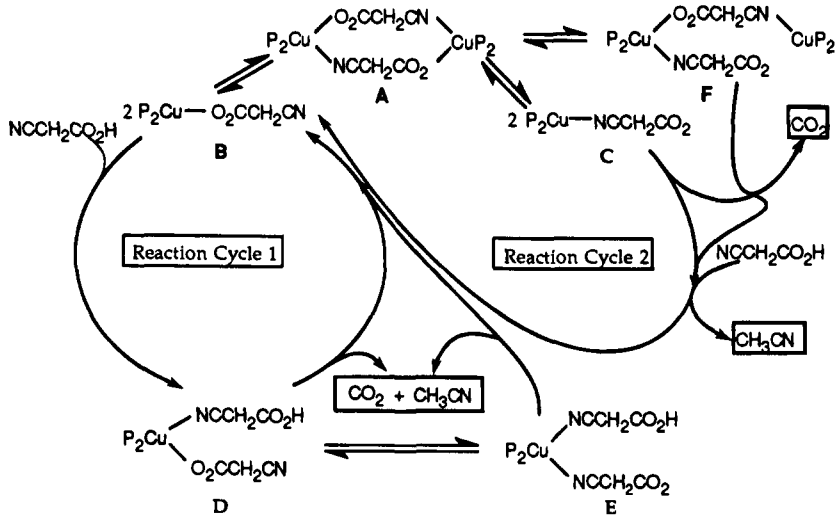

coordinate both in solution and in the solid state, whereas, in all cases, isolation of bis(triphenylphosphine)copper(I) cyanoacetates has resulted in coordinatively saturated copper(I) complexes. Complexes **A**, **B**, and **E** presented in Scheme 1 have been isolated and characterized by X-ray crystallography. In complexes **A** and **E**, P equals triphenylphosphine, and in complex **B**, P equals the much bulkier tricyclohexylphosphine ligand. The most notable mechanistic aspect of Scheme 1 is that the rate-determining step in both $^{13}CO_2$ exchange and catalytic decarboxylation (in the low [acid] regime) is CO_2 loss from an intermediate(s) containing a cyanoacetate ligand bound to copper(I) *via* the nitrile functionality. That is, the decarboxylation reaction is inhibited by CO_2 and is zero-order in cyanoacetic acid at modest concentrations. Acetonitrile was also shown to inhibit the decarboxylation process in the presence of copper(I). Indeed, the reaction is not catalyzed by copper(I) species in acetonitrile solvent due to the propensity of CH_3CN to bind copper(I) blocking the nitrile binding site of cyanoacetate. At higher acid concentrations, species such as **D** and **E** become more important, with decarboxylation occurring, albeit somewhat more slowly, by these intermediates in the same manner as has been exhaustively described in more stable tungsten carbonyl derivatives. Intra- and/or intermolecular hydrogen bonding is likely responsible for retarding the decarboxylation step as is seen when using the free cyanoacetate ion as catalyst. In this instance, $^{13}CO_2$ exchange is ~10 times faster than decarboxylation where $O_2CCH_2CN/HOOCCH_2CN$ is strongly hydrogen-bonded.

The concentration dependence of the decarboxylation and CO_2 exchange process on the nature of the phosphine ligand is best accounted for by enhanced $Cu-NCCH_2CO_2$ interaction in a $Cu(PPh_3)_3NCCH_2CO_2$ derivative and a corresponding decrease in such interaction in the sterically crowded $Cu(Cy_3P)_3^+\cdots NCCH_2CO_2^-$ derivative. In this latter instance, the bulky tricyclohexylphosphine ligand may inhibit cyano-coordination in contrast to the less basic and smaller triphenylphosphine upon addition of excess phosphine. These differences can account for the divergent behavior noted upon addition of excess phosphine during catalysis, (Figures 9a and b). Furthermore, Scheme 1 accounts for why phosphine copper(I) cyanoacetate undergoes reversible decarboxylation, whereas pentacarbonyltungsten(0) cyanoacetate does not. Tungsten(0) cyanoacetate forms very stable W–O bonds with carboxylates, and the carboxylate ligands do not readily dissociate in solution.[4] The difference in these two systems lies in the ability of copper(I) to dissociate easily, allowing for the formation of various nitrile-bound copper(I) derivatives in solution. Tungsten(0)'s coordination sphere is rigid when compared to the versatile nature of copper(I). Indeed, the rate-limiting step for the tungsten(0) catalyst was determined to be CO loss accompanied by cyanoacetic acid binding through the nitrile functionality.[4] Importantly, CO_2 loss did not occur *via* an interaction of CO_2 with the metal center. Basic phosphines promote carboxylate dissociation in the electronically saturated copper(I) complexes and, therefore, promote reversible decarboxylation.

Based on the compilation of our observations, we hypothesized that copper(I)'s role is to simply enhance the decarboxylation rate *via* an electrophilic interaction. That intermediates, such as **C** and **E**, are unstable with respect to decarboxylation is seen in the elongated C–C bonds in O_2C-CH_2CN upon CN coordination to the copper(I) center (Table 2). Comparable C–C bond lengths in complexes **3** and **5**, where the cyanoacetate ligand is monodentate-bound by the carboxylate functionality, are significantly longer than those of complex **1**. Similarly, Steinberger and Westheimer have proposed a mechanism involving electrophilic catalysis for the decarboxylation of dimethyloxaloacetic acid.[26] These studies showed that a variety of heavy metal ions were active catalysts, albeit copper(II) was the best. In an effort to further test our hypothesis, we prepared several zinc(II) complexes and tested them for catalytic activity. Examination of Zn–O bond distances of various zinc carboxylates with nitrogen donor ligands reveals that neutral bidentate and tridentate amine ligands that are coordinated to zinc(II) promote longer Zn–O bonds,[27–30] when compared to charged (hydrotris(pyrazoyl)borate)zinc(II) carboxylates.[20,23] As mentioned earlier, we found that (1,5,9-triazacyclododecane)(Zn)(O_2CCH_3)[Ph_4B] was a superior catalyst to (hydrotris(3-phenylpyrazole)borate)(Zn) cyanoacetate. The zinc(II) catalysts are inferior to copper(I) catalysts but superior to the previously mentioned tungsten(0) catalyst. Zinc(II) is a harder acid than copper(I) and binds more strongly to the carboxylate functionality, thus leading to slower decarboxylation rates. The decarboxylations of cyanoacetic acid using the different metal systems, copper(I) and zinc(II), have similar kinetic features and appear to occur

(26) Steinberger, R.; Westheimer, F. H. *J. Am. Chem. Soc.* **1951**, *73*, 429.
(27) Reibenspies, J. H.; Holtcamp, M. W.; Khandelwal, B.; Darensbourg, D. J. *Z. Kristallogr.*, in press.
(28) Kirchner, C.; Krebs, B. *Inorg. Chem.* **1987**, *26*, 3569.
(29) Ahlgren, M.; Turpeinen, U.; Hamalainen, R. *Acta Chem. Scand., Ser. A* **1982**, *36*, 841.
(30) Chaudhuri, P.; Stockeim, C.; Wieghardt, K.; Deck, W.; Gregorzik, R.; Vahrenkamp, H.; Nuber, B.; Weiss, J. *Inorg. Chem.* **1992**, *31*, 1451.

by analogous decarboxylation mechanisms. These observations are only consistent with electrophilic catalysis.

Although the insertion reaction depicted in eq 8 has been described as proceeding *via* a transition state as indicated in Chart 1, there is *no* experimental evidence to substantiate such a process.[31-33] That is, unlike the insertion of CO_2 into the W−R

$$(R_3P)_2CuR + CO_2 \rightarrow (R_3P)_2CuO_2CR \quad (8)$$

Chart 1

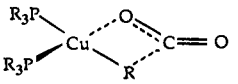

bond where definitive evidence has been presented for a transition state analogous to that in Chart 1,[34,35] no confirmation of this in the copper(I) systems is available. The early observations of Tsuda and co-workers,[2a] where it was found that the addition of 3 equiv of phosphine ligands to cuprous cyanomethyl promoted reversible CO_2 uptake, might easily be explained by means of an ionic mechanism (Scheme 2). In this instance, the Cu−R bond would be highly distorted or heterolytically cleaved. Indeed, it has been demonstrated that copper(I) complexes with more basic phosphine ligands exhibit $\nu(Cu-CH_3)$ vibrations at lower frequency and have lower activation energies for thermolysis than those with less basic phosphines.[36] In other words, phosphines should promote heterolytic Cu−R bond disruption as indicated in Scheme 2.

Scheme 2

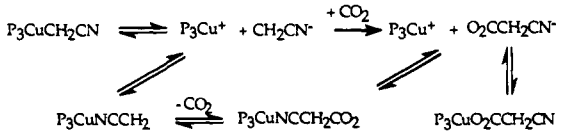

Concluding Remarks

Copper(I) derivatives of carboxylic acids, which are more effective catalysts for the decarboxylation of the corresponding organic acid to the respective hydrocarbon and CO_2 than the conjugate base of that acid alone, do so *via* a mechanism that involves electrophilic catalysis. That is, at this time there is no conclusive evidence that supports a direct interaction of CO_2 with the copper(I) center during the CO_2 insertion/deinsertion involving a Cu−R bond (Chart 1). In particular, a consistent mechanistic perspective for the homogeneous catalytic decarboxylation of cyanoacetic acid utilizing a variety of metal (tungsten(0), copper(I), and zinc(II)) complexes can now be represented. Furthermore, this viewpoint is completely consistent with the mechanistic pathway for the coupling of substrates containing acidic C−H bonds and CO_2 in the presence of electron-rich transition metal complexes.[37,38]

Acknowledgment. Financial support of this research by the National Science Foundation (Grant 91-19737) and the Robert A. Welch Foundation is greatly appreciated.

Supplementary Material Available: ORTEP views of molecules **1a** and **1b**, including molecules of solvation. Tables providing complete listings of atomic coordinates, bond lengths, bond angles, anisotropic thermal parameters, H-atom coordinates, and isotropic displacement parameters for complexes **3**, **4**, and **5** (34 pages). This material is contained in many libraries on microfiche, immediately follows this article in the microfilm version of the journal, and can be ordered from the ACS; see any current masthead page for ordering information.

JA942750C

(31) Sakaki, S.; Ohkubo, K. *Inorg. Chem.* **1988**, *27*, 2020.
(32) Sakaki, S.; Ohkubo, K. *Inorg. Chem.* **1989**, *28*, 2583.
(33) Sakaki, S.; Ohkubo, K. *Organometallics* **1989**, *8*, 2970.
(34) Darensbourg, D. J.; Hanckel, R. K.; Bauch, C. G.; Pala, M.; Simmons, D.; White, J. N. *J. Am. Chem. Soc.* **1985**, *107*, 7463.
(35) Darensbourg, D. J.; Grötsch, G. *J. Am. Chem. Soc.* **1985**, *107*, 7473.
(36) Miyashita, A.; Yamamoto, T.; Yamamoto, A. *Bull. Chem. Soc. Jpn.* **1977**, *50*, 1109.
(37) (a) Behr, A.; Herdtweck, E.; Herrmann, W. A.; Keim, W.; Kipshagen, W. *Organometallics* **1987**, *6*, 2307. (b) Reference 1c, p 66. (c) English, A. D.; Herskovitz, T. *J. Am. Chem. Soc.* **1977**, *99*, 1648. (d) Ittel, S. D.; Tolman, C. A.; English, A. D.; Jesson, J. P. *J. Am. Chem. Soc.* **1978**, *100*, 7577.
(38) Fukue, Y.; Oi, S.; Inoue, Y. *J. Chem. Soc., Chem. Commun.* **1994**, 2091.